THE CRUSTAL AND MANTLE VELOCITY STRUCTURE IN CENTRAL ASIA FROM 3D TRAVEL TIME TOMOGRAPHY

Randolph J. Martin[1], Levent Gulen[2], Youshun Sun[2], M. Nafi Toksöz[2]

New England Research[1] and Massachusetts Institute of Technology[2]

Sponsored by the National Nuclear Security Administration

Award No. DE-AC52-08NA28751

ABSTRACT

The lithospheric structure in Central Asia features large blocks such as the Indian plate, the Afghan block, the Turan plate, and the Tarim block. This geologically and tectonically complicated area is also one of the most seismically active regions in the world. We developed *P*- and *S*-wave velocity structures of Central Asia in the crust using the travel-time data from Kyrgyzstan, Tajikistan, Kazakhstan, and Uzbek Republic. We chose the events and stations between 32N65E and 45N85E and focused on the areas of Pamir and western Tianshan. In this data set, there are more than 6000 *P* and *S* arrivals received at 80 stations from about 300 events. Double difference tomography is applied to relocate events and to determine seismic velocities simultaneously. Our results provide an improved earthquake location and high resolution crustal structure in this region.

To extend the model deeper into the mantle through the upper mantle transition zone, ISC/EHB data for *P* and *PP* phases are combined with the ABCE data. To counteract the "smearing effect," the crust and upper mantle velocity structure, derived from regional travel-times, is used. An adaptive grid method based on ray density is used in the inversion. Regional teleseismic tomography provides a high-resolution, 3-D *P*-wave velocity model for the crust, upper mantle, and the transition zone. The crustal models correlate well with geologic and tectonic features. The upper mantle tomograms show the images of Tian Shan. The slab geometry is quite complex, reflecting the history of the changes in the plate motions.

OBJECTIVES

The main goal of this project is to develop a database consisting of: new waveform data, seismic event catalogs, and information on the geology and active tectonics in the Central Asian region. Over the past years, we have collected geologic, geophysical, seismic event catalog and phase arrival data from local networks in the Caucasus region; this project extends the work into the CASRI (Central Asia Seismic Research Initiative) region (Kazakhstan, Kyrgyzstan, Uzbekistan, and Tajikistan). The new database is crucial in generating a detailed crust and mantle structure model and characterizing seismic wave propagation and attenuation in Central Asia. The local seismic networks, calibration events, improved crust and mantle structure models and better location algorithms (e.g., multiple-event grid search, double difference methods) will improve the event locations. This new database will form the basis for mitigating earthquake hazard in Central Asia, and it will aid in the monitoring of these regions of strategic interest to U.S. national security.

RESEARCH ACCOMPLISHED

The Regional Tectonic Setting

The active tectonics of Asia is predominantly the result of the continental collision and the continuing continental convergence between the Indian and the Eurasian Plates. As a result, large scale structures such as the Himalayas, Tibet, Hindu Kush-Pamir, and Zagros have been produced by the collision and the post-collisional convergence.

The India-Eurasia collision is also accommodated by major thrusting and crustal shortening as evidenced by the high elevation and compressional structures such as the Himalayas, Hindu Kush-Pamir, and the Tien Shan and Zagros region (Figure 1). An alternative model suggesting that the mode of continental deformation can be explained by continuum mechanics was proposed to explain the continental deformation of Asia (England and Houseman, 1986; Houseman and England, 1993). This alternative model assumes that the collision and convergence of the Indian and Eurasian Plates are mainly accommodated by lithospheric thickening, and the resultant increased gravitational body forces drive the active tectonics of Asia. The Global Positioning System measurements and crustal rheology modeling in Asia provide evidence that the deformation in the shallow brittle crust occurs on a distributed network of faults, and some regions, such as the Tarim Basin, the Ordos and South China, behave as rigid blocks; however, deformation of a continuous medium at depth is the best description of the present day tectonics of Asia (Royden et al., 1997; Wang et al., 2001; Calais et al., 2003; Zhang and Gan, 2008). The *Pn* and *Sn* tomographic models (Figure 1) show the heterogeneities below the crust that correlate well with the subduction zones, rigid blocks and other tectonic features.

The countries that are within the interest area of the CASRI project are primarily affected by the tectonic deformations and associated seismic activity of the Tien Shan and the Pamir-Hindu Kush regions. Since we have covered the Neotectonic analysis of the Tien Shan region previously (Martin et al., 2009) we will briefly summarize the active tectonics of the Pamir-Hindu Kush region in this paper.

The Pamir-Hindu Kush Region

The Pamir-Hindu Kush region is located at the western syntaxis of the Himalayan belt and it has an elevation of 4000–5000 m. This orojenic syntaxis consists of several terrains that were accreted to the southern margin of Asia during the Paleozoic-Mesozoic closure of the Tethys Ocean (Tapponnier et al., 1981; Burtman and Molnar, 1993; Yin and Harrison, 2000; Schwab et al., 2004; Robinson et al., 2007). Before the India-Asia continental collision took place about 45–50 my ago, the Pamir region was an Andean-style plate margin. The post-collisional indentation of the Indian Plate into the Eurasian Plate caused intense deformation and crustal shortening and created major thrusts and strike-slip faults bounding the region (Figure 2). The Main Pamir Thrust forms the northern boundary separating the Pamirs from the Tien Shan. The left-lateral strike-slip Darvaz-Karakul Fault Zone marks the boundary in the west between the Tadjik Depression and the Pamirs. The right-lateral strike-slip Karakorum fault zone forms the eastern boundary that separates the Pamirs from the western Kunlun and the Tarim Basin (Molnar and Tapponnier, 1978). The Main Pamir Thrust has been interpreted to have accommodated about 300 km of crustal shortening, and additionally, at least 300 km of shortening was also accommodated internally by thrusting and faulting within the Pamirs during the Cenozoic (Burtman and Molnar, 1993).

The Pamir-Hindu Kush region has high seismic activity and many large earthquakes have occurred in the region. The focal mechanism solutions for the earthquakes in this region indicate predominantly thrust events, as would be expected, and some strike-slip events along major shear zones that form the boundaries of the region.

The most interesting aspect of the Pamir-Hindu Kush seismicity is that this region is one of the most active regions of intermediate depth seismicity. Many studies have been carried out to evaluate the seismicity of the Pamir-Hindu Kush region (Chatelain et al., 1980; Roecker 1982; Fan and Ni, 1989; Burtman and Molnar, 1993; Fan et al., 1994; Pegler and Das, 1998). More recently, seismic tomographic studies of the mantle structure beneath the Pamir-Hindu Kush region have revealed that the intermediate depth seismicity is the result of the existence of two opposing sense subduction zones (Freiderich, 2003; Kumar et al., 2005; Koulakov and Sobolev, 2006; Negredo et al., 2007). The Indian lithosphere subducts steeply northward beneath the Hindu Kush, and the Asian lithosphere subducts southward beneath the Pamirs; the interface of the two converging lithospheres, at mantle depths beneath the Pamir-Hindu Kush region, forms the zone of intermediate depth seismicity.

Travel-Time Data

An important task under this project is to collect arrival time data from seismic stations situated in the Central Asia. A significant number of these stations are in networks whose data are not available from global data centers such as IRIS (Incorporated Research Institutions for Seismology) or ISC (International Seismological Centre). Figure 3 shows seismic stations in the region from which we have obtained data either through data centers or by bilateral arrangements. In the previous studies of this region, teleseismic data and surface wave data were the main data sources. Although teleseismic data provide us with much information about the mantle, shallow structure is still unclear. The horizontal resolution is also limited by available periods of surface waves. Therefore, we use the local and regional travel times to invert for the 3-D crustal velocity structure in this region. We selected the stations and events between 32°N-65°E and 45°N-85°E where there are 68 stations and 220 events (Figure 3). More than 2200 P-wave phase picks are employed in the inversion. The average grid spacing is 100 km and the inverted grids lay on six layers. The source-station ray paths are also shown in Figure 3 and the ray density is dense enough to obtain good tomographic resolution.

***P*- and *S*-Wave Travel-Time Tomography of the Crust and Upper Mantle**

A high-resolution tomographic model for the heterogeneous crust is constructed by iterative, non-linear tomography. To generate adequate starting models for the nonlinear inversion, we combine pertinent information from global (Mooney et al., 1998; Stevens et al., 2001; Ritzwoller et al., 2002), regional, and local crust and uppermost mantle models. Next, we use the adaptive moving window (AMW) approach (Sun et al., 2004, 2008) to obtain crustal velocities and *Pn* and *Sn* models from a 1-D Monte Carlo inversion of local ($\leq 20°$) arrival time data in the whole region, building these into the next model (Model #2). The third step is a tomographic inversion of the local and regional arrival time data for 3-D variations in the *P*- and *S*-wave speed, using Model #2 as the initial input model.

For this purpose we use a modified version of Zhao's tomographic method (Zhao et al., 1992, 1994; Zhao, 2001; Sun and Toksöz, 2006), which allows for 3-D velocity variations everywhere in the model and can accommodate velocity discontinuities. The velocity structure is discretized using a 3-D grid. The velocity perturbation at each point is calculated by linear interpolation of the velocity perturbations at surrounding (adjacent) grid nodes. The velocity perturbations at grid nodes are the unknown parameters for the inversion procedure. To calculate travel-times and ray paths accurately and rapidly, the pseudo-bending technique (Um and Thurber, 1987) is used iteratively. We correct for station elevations by including station correction terms in the inversion. The nonlinear tomographic problem is solved by repeated linear inversions. At each iteration, perturbations to hypocentral parameters and velocity structure are determined simultaneously.

Starting from the *P* and *S* models obtained from the above strategy, we apply an adaptive-mesh double-difference tomography method to the newly assembled data set to further improve event locations and velocity models (Zhang and Thurber, 2003; 2006). In this approach, the configuration of model cells is adjusted to sampling density to stabilize the inversion and (locally) optimize spatial resolution. Figure 4 shows the *P* and *S* travel-time, distance graphs, and *P*-wave travel-time residual distribution before and after the 3-D inversion. The standard deviation improved from 2.1 seconds to 0.9 seconds as a result of the 3-D inversion.

Figure 5 shows *Pn* and *Sn* structure and Figures 6 and 7 show the tomographic results obtained for the Central Asian crustal structure. Since most phase arrivals are *Pn*, the layers around the Moho (50 km and 70 km) are imaged with the best resolution. In addition, the shallower structure can also be recovered along the China boundary. Figure 8 shows the upper mantle velocity structure at the depths of 100, 200, 400, and 600 km obtained by the double difference tomography method.

CONCLUSIONS

Our results show strong crust and mantle heterogeneities in Central Asia. The low velocity zones are found near the Tien Shan, northern Pamirs, and Tajik depression, whereas high velocity anomalies exist beneath the southern Pamir, Kazakh shield, and the Tarim basin. High velocities delineate the subduction zones and active or fossil slabs.

The Moho depth in the region is about 70 km. There are areas such as the western Tarim Basin where the Moho discontinuity is much shallower

The extension of the velocity models into the mantle transition zone is accomplished by adding the teleseismic data from the 1964–2008 ISC/EHB database, which contains over 10 million P-wave travel-times, and from datasets obtained by the various national data centers.

REFERENCES

Burtman, V. S. and P. Molnar (1993). Geological and geophysical evidence for deep subduction of continental crust beneath the Pamir, *Geol. Soc. Am. Spec. Paper* 281, 76 p.

Calais, E., M. Vergnolle, V. San'kov, A. Lukhnev, A. Miroshnitchenko, S. Amarjargal, and J. Déverchère (2003). GPS measurements of crustal deformation in the Baikal-Mongolia area (1994-2002): Implications for current kinematics of Asia, *J. Geophys. Res.* 108: doi:10.1029/2002JB002373.

Chatelain, J. L., S. W. Roecker, D. Hatzfeld, and P. Molnar (1980). Microearthquake seismicity and fault plane solutions in the Hindu Kush region and their tectonic implications, *J. Geophys. Res.* 85: 1365–1387.

England, P. and G. Houseman (1986). Finite strain calculations of continental deformation: 2. Comparison with the India-Eurasia collision zone, *J. Geophys. Res.* 91: 3664–3676.

Fan, G. and J. F. Ni (1989). Source parameters of the 13 February Karakoram earthquake, *Bull. Seismol. Soc. Am.* 79: 945–954.

Fan, G., J. F. Ni, and T. C. Wallace (1994). Active tectonics of the Pamirs and Karakorum, *J. Geophys. Res.* 99: 7131–7160.

Friederich, W. (2003). The S-velocity structure of the east Asian mantle from inversion of shear and surface waveforms, *Geophys. J. Int*. 153: 88–102.

Houseman, G. and P. England (1993). Crustal thickening versus lateral expulsion in the India-Asia continental collision, *J. Geophys. Res.* 98: 12,233–12,249.

Koulakov, I. S. and V. Sobolev (2006). A tomographic image of Indian lithosphere break-off beneath the Pamir-Hindukush region, *Geophys. J. Int*. 164: 425–440.

Kumar, P., X. Yuan, R. Kind, G. L. Kosarev (2005). The lithosphere-asthenosphere boundary in the Tien Shan-Karakoram region from S receiver functions: Evidence for continental subduction, *Geophys. Res. Lett.* 32: doi: 10.1029/2004GL022291.

Martin, R. J., M. N. Toksoz, L. Gulen, Y. Sun (2009). Extension of the CauSIN Study into Central Asia: Final Report, Contract No. De-AC52-04NA25612.

Molnar, P. and P. Tapponnier (1978) Active tectonics of Tibet, *J. Geophys. Res*. 83: 5361–5375.

Mooney, W.D., G. Laske, and G. Masters (1998). CRUST 5.1: A global crustal model at 5°× 5°, *J. Geophys. Res*. 103: 727–747.

Negredo, A. M., A. Replumaz, A. Villasenor, and S. Guillot (2007). Modeling the evolution of continental subduction process in the Pamir-Hindu Kush region, *Earth Planet. Sci. Lett*. 259: 212225.

Pegler, G. and S. Das (1998). An enhanced image of the Pamir-Hindu Kush seismic zone from relocated earthquake hypocenters, *Geophys. J. Int*. 134: 573–595.

Ritzwoller, M.H., M. P. Barmin, A. Villasenor, A. L. Levshin, and E. R. Engdahl (2002). Pn and Sn tomography across Eurasia to improve regional seismic event locations, *Tectonophysics* 358: 39-55.

Robinson, A. C., A. Yin, C. E. Manning, T. M. Harrison, S. H. Zhang, and X. F. Wang (2007). Cenozoic evolution of the eastern Pamir: Implications for strain-accommodation mechanisms at the western end of the Himalayan-Tibetan orogen, *Geol. Soc. Am. Bull*. 119: doi: 10.1130/B25981.1

Roecker, S. W. (1982). Velocity structure of the Pamir-Hindu Kush region: possible evidence of subducted crust, *J. Geophys. Res*. 87: 945–959.

Royden, L.H., B.C. Burchfiel, R.W. King, E. Wang, Z. Chen, F. Shen, and L. Yuping (1997). Surface deformation and lower crustal flow in eastern Tibet, *Science* 276: 788–790.

Schwab, M., L. Ratschbacher, W. Siebel, M. McWilliams, V. Minaev, V. Lutkov, F. Chen, K. Stanek, B. Nelson, W. Frisch, and J. L. Wooden (2004). Assembly of the Pamirs: Age and origin of magmatic belts from the southern Tien Shan to the southern Pamirs and their relation to Tibet, *Tectonics* 23: doi:1029/2003TC001583.

Stevens, J. L., D. A. Adams, and G. E. Baker (2001). Improved surface wave detection and measurement using phase-matched filtering with a global one-degree dispersion model, in *Proceedings of the 23rd Seismic Research Review: Worldwide Monitoring of Nuclear Explosions*, LA-UR-01-4454, Vol. 1, pp. 420–430.

Sun, Y., L. Xu, S. Kuleli, F. D. Morgan, and M. N. Toksöz (2004). Adaptive moving window method for 3-D P-velocity tomography and its application in China, *Bull. Seismol. Soc. Am*. 94: 740–746.

Sun, Y. and M. N. Toksöz (2006). Crustal structure of China and surrounding regions from P wave traveltime tomography, *J. Geophys. Res*. 111: doi:10.1029/2005JB003962.

Sun, Y., M. N. Toksöz, S. Pei, D. Zhao, F. D. Morgan, and A. Rosca (2008). S-wave tomography of the crust and uppermost mantle in China, *J. Geophys. Res*. 113: doi:10.1029/2008JB005836.

Tapponnier, P., M. Mattauer, F. Proust, and C. Cassaigneau (1981). Mesozoic ophiolites, sutures, and large scale tectonic movements in Afghanistan, *Earth Planet. Sci. Lett*. 52: 355–371.

Um, J. and C. Thurber (1987). A fast algorithm for two-point seismic ray tracing, *Bull. Seismol. Soc. Am*. 77: 972–986.

Wang, Q. P. Zhang, J. T. Freymueller, R. Bilham, K. M. Larson, X. Lai, X. You, Z. Niu, J. Wu, Y. Li, J. Liu, Z. Yang, and Q. Chen (2001). Present-day crustal deformation in China constrained by Global Positioning System measurements, *Science* 294: 574–577.

Yin, A. and T. M. Harrison (2000). Geologic evolution of the Himalayan-Tibetan Orogen, Annu. Rev. *Earth Planet. Sci*. 28: 211–280.

Zhang, H. and C. Thurber (2003). Double-Difference Tomography: The Method and Its Application to the Hayward Fault, California, *Bull. Seismol. Soc. Am*. 93: doi: 10.1785/0120020190.

Zhang, H. and C. Thurber (2006). Development and applications of double-difference tomography, *Pure Appl. Geophys*. 163: doi:10.1007/s00024-005-0021-y.

Zhang, P.-Zh. and W. Gan (2008). Combined model of rigid-block motion with continuous deformation: Patterns of present-day deformation in continental China, in Burchfiel, B.C., and Wang, E., Eds., Investigations into the Tectonics of the Tibetan Plateau, *Geol. Soc. Am*. Special Paper 444, 59–71, doi:10.1130/2008.2444.

Zhao, D. (2001). Seismic structure and origin of hotspots and mantle plumes, *Earth Planet. Sci. Lett*. 192: 251–265.

Zhao, D., A. Hasewaga, and S. Horiuchi (1992). Tomographic imaging of P and S wave velocity structure beneath northeastern Japan, *J. Geophys. Res*. 97: 19909–19928.

Zhao, D., A. Hasegawa, and H. Kanamori (1994). Deep structure of Japan subduction zone as derived from local, regional and teleseismic events, *J. Geophys. Res*. 99: 22313–22329.

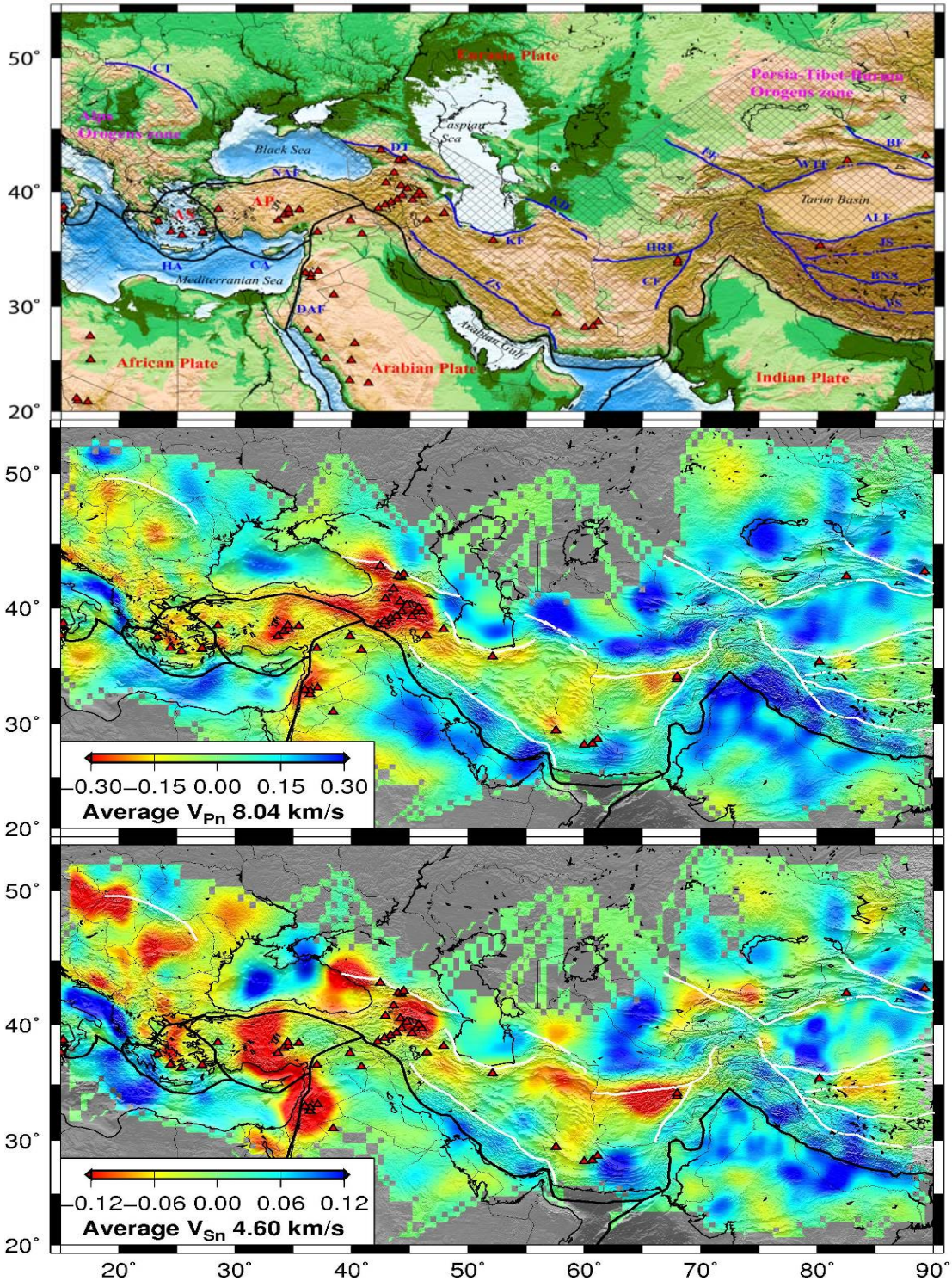

Figure 1. Simplified tectonic map (top) and imaged *Pn* (middle) and *Sn* velocity lateral variations from Alps to Himalaya region. The dark lines show the plate boundaries and the red triangles are volcanoes. ALF: Altyn fault; AF: Anatolian Fault; AP: Anatolian plate; AS: Aegean sea plate; BF: Boluokenu fault; BNS: Bangong-Nujiang suture; CA: Cyprean arc; CF: Chaman fault; CT: Capathians thrust belt; DSF: Dead Sea Fault; DT: Dagestan thrust belt; FF: Fergana Fault; HA: Hellenic arc; HRT: Hari Rod fault; KD: Kopeh Dagh fault; JS: Jinsha river suture; KF: Khazar fault; WTF: Western Tianshan faults; YS: Yalong-zangbo suture; ZS: Zagros Suture.

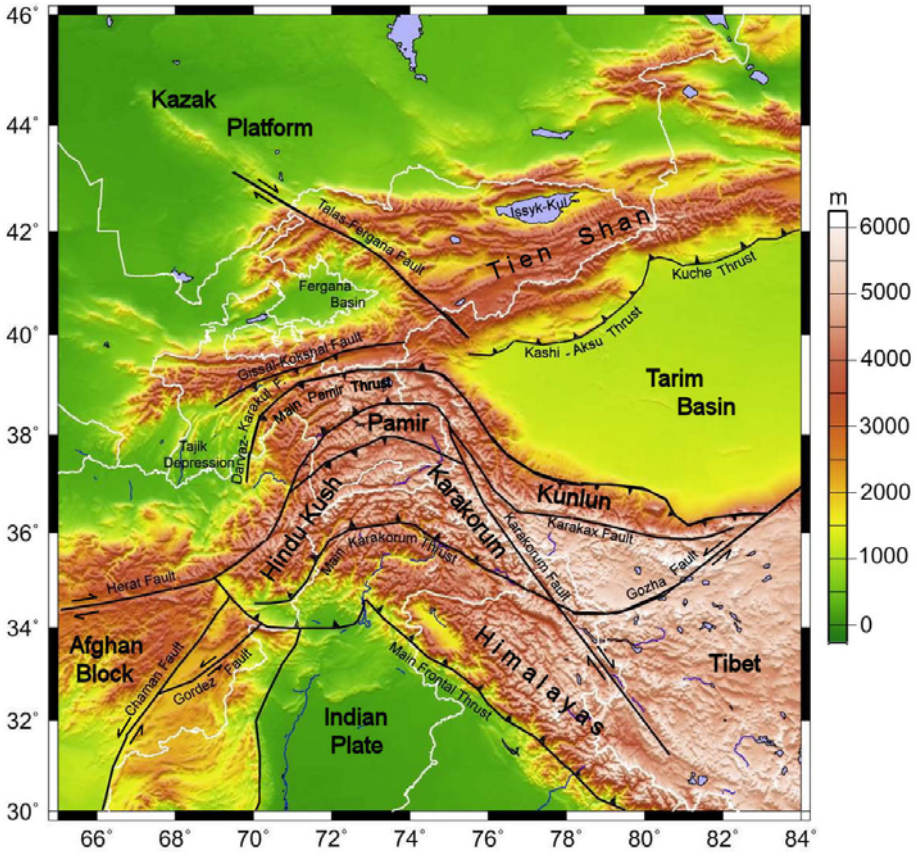

Figure 2. Map of the Pamir-Hindu Kush and surrounding areas showing major tectonic features.

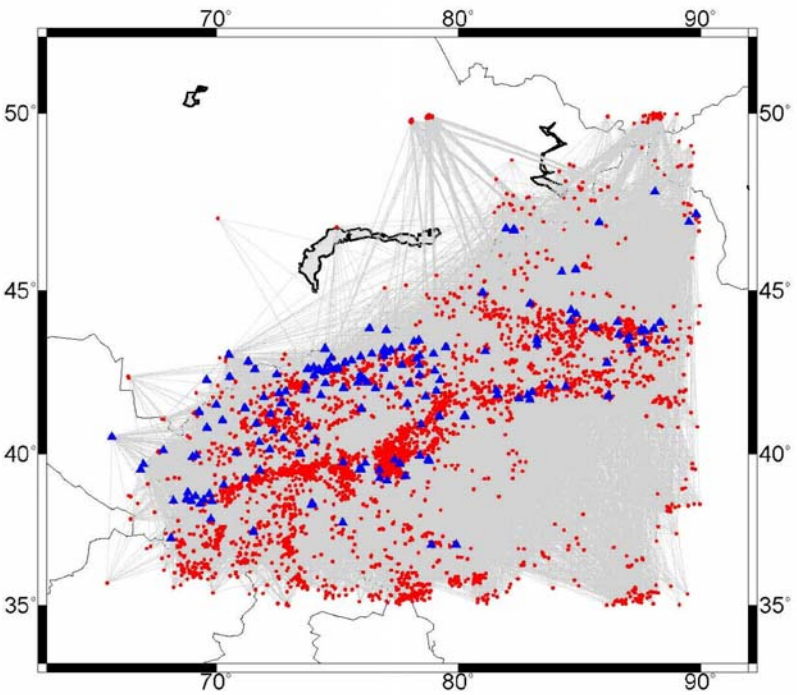

Figure 3. Ray path distribution in Central Asia. The stations are shown with blue triangles and the events are shown with red dots.

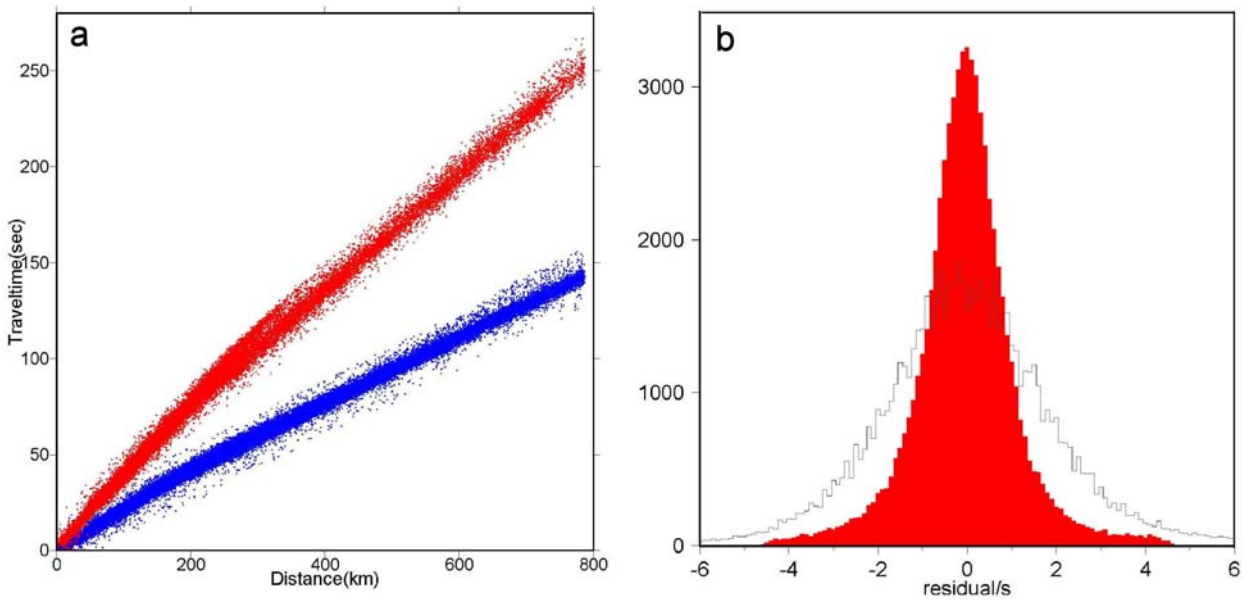

Figure 4. (a) *P* and *S* travel time distribution in the study area. (b) *P*-wave travel time residual distribution before and after (red) 3-D inversion. The standard deviation decreased from 2.1 seconds to 0.9 seconds.

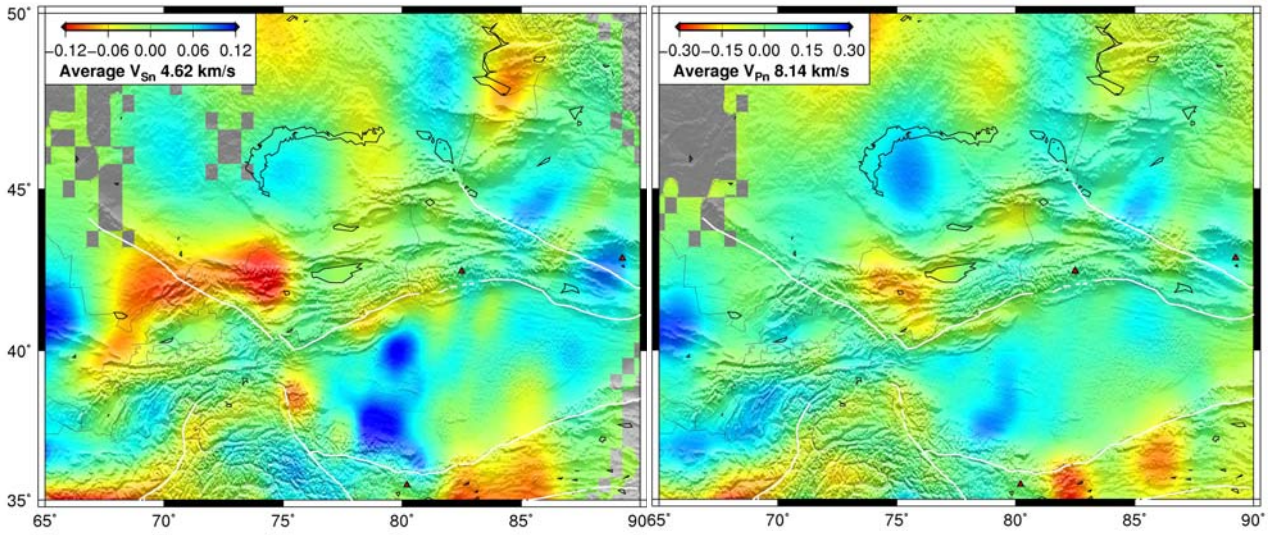

Figure 5. Imaged *Pn* (left) and *Sn* velocity lateral variations of the Central Asia region.

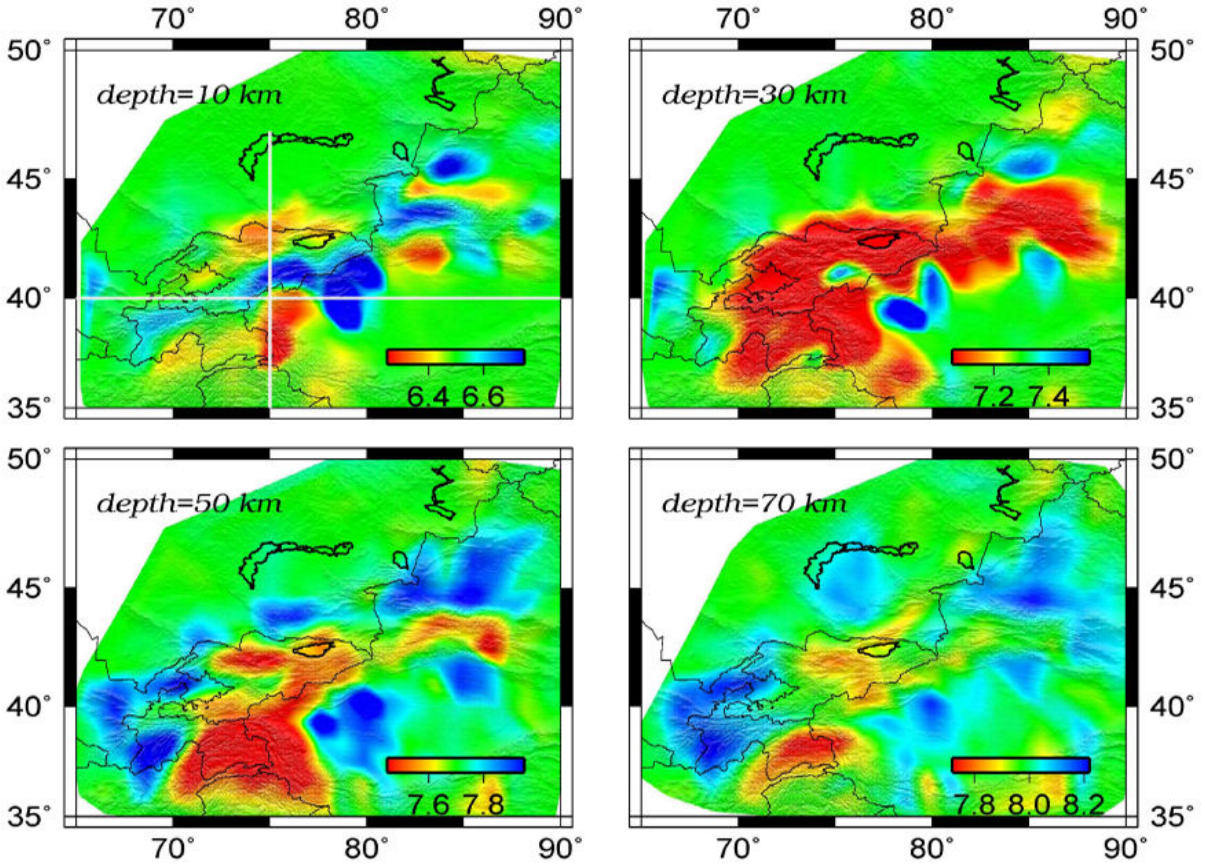

Figure 6. 3-D P-wave velocity structure for different depths in Central Asia. These maps were generated by assuming different P-wave reference velocities for each depth.

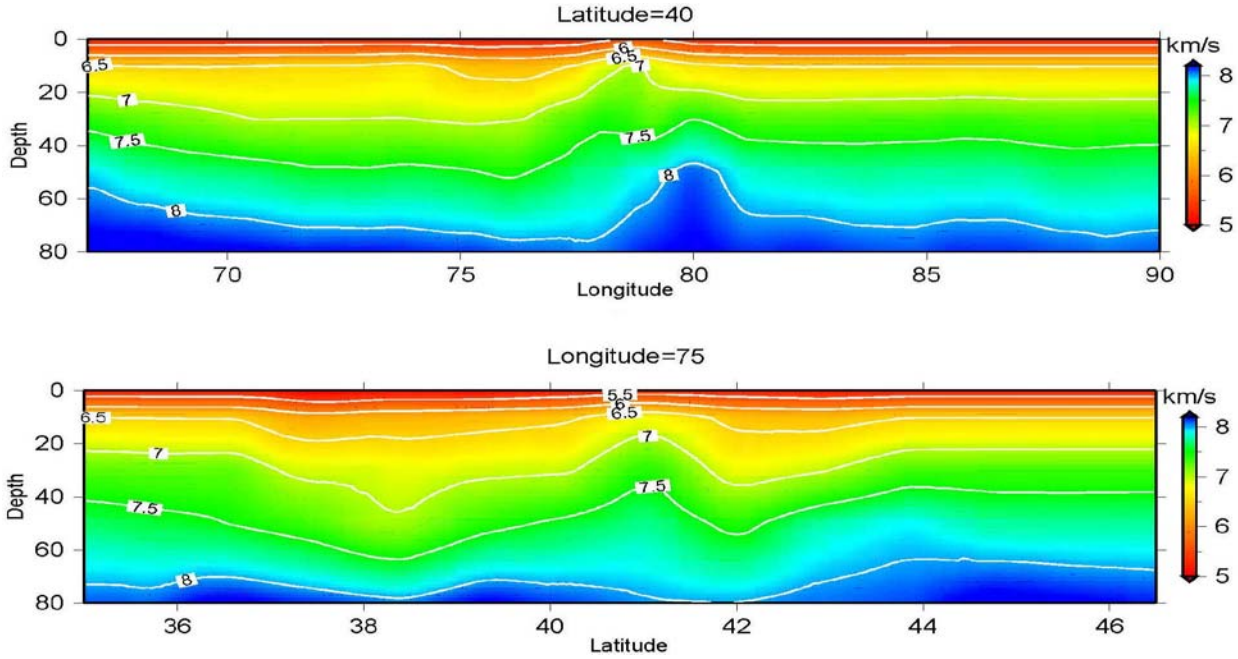

Figure 7. Vertical velocity profiles (the locations are shown in Figure 6).

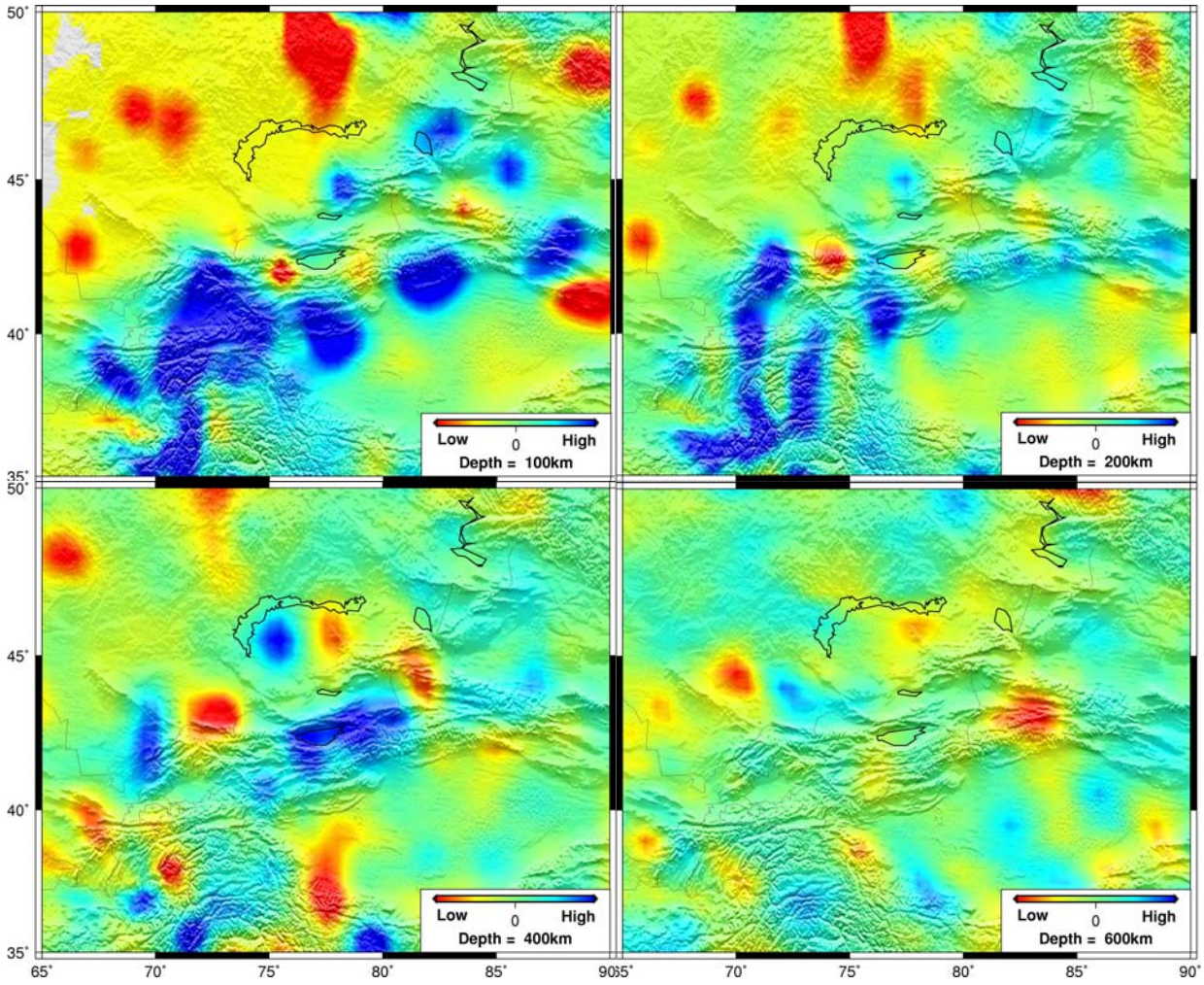

Figure 8. Upper mantle velocity structure at the depths of 100, 200, 400, and 600 km obtained by the double difference tomography method.